Interaction Between One-dimensional Dark Spatial Solitons and Semi-infinite Dark Stripes

Peter Hansinger[a], Georgi Maleshkov[b], Nasko Gorunski[b], Nikolay Dimitrov[b], Alexander Dreischuh[b,*], Gerhard G. Paulus[a,c]

[a] *Institute for Optics and Quantum Electronics, Faculty of Physics and Astronomy, Friedrich-Schiller-University, Max-Wien-Platz 1, D-07743 Jena, Germany*
[b] *Department of Quantum Electronics, Faculty of Physics, Sofia University, 5, J. Bourchier Blvd., Sofia-1164, Bulgaria*
[c] *Helmholtz-Institute Jena, Helmholtzweg 4, D-07743 Jena, Germany*

Abstract

In this work we numerically study the evolution and interaction of one-dimensional (1-D) dark spatial solitons and semi-infinite dark stripes (SIDSs) in a local self-defocusing Kerr nonlinear medium. The experimental results in the linear regime of propagation confirm that the SIDS bending and fusion with the infinite 1-D dark beam modeled for negative nonlinearity is due to the opposite phase semi-helicities of SID beam ends. Results for several interaction scenaria show that bending ends of the semi-infinite dark stripes splice to the 1-D dark beam to form structures resembling waveguide couplers/branchers. Well pronounced modulational stability of 1-D dark spatial solitons under strong symmetric background beam modulation from decaying SIDSs is predicted.

Keywords: Kerr nonlinearity, self-defocusing, phase dislocation, dark spatial soliton, semi-infinite dark beam, all-optical interaction, all-optical guiding
PACS: 42.65.Tg, 42.65.Wi, 42.65.Jx, 42.65.Hw

---

*Corresponding author. Tel.: (+359 2) 8161 611; fax: (+359 2) 868 89 13.
Email address: ald@phys.uni-sofia.bg (Alexander Dreischuh)

1. Introduction

Optical vortices (OVs) [1] and one-dimensional dark beams [2] with their characteristic helical and step-like phase profiles [3] are classical entities in the field of singular optics [4]. Due to the presence of a two-dimensional (2-D) point phase dislocation on the axis of the OVs and the presence of a one-dimensional (1-D) phase dislocation along a line for the 1-D dark beam, the phase of the optical field becomes indeterminate and the field amplitude vanishes at the dislocation point(s) [5]. It is known that the relative phases of interacting singular beams determine their coherent interaction in both the linear and the locally nonlinear propagation regime [6, 7, 8]. This also holds when singular beams are arranged to form optical lattices [9, 10].

Propagation of optical beams in nonlinear media (NLM) has been a subject of continuing interest for more than four decades due to the possibility for creation of reconfigurable waveguides through the intensity-dependent refractive index change [11, 12]. Such optically induced waveguides can guide weak signal beams and pulses [13, 14], which motivates the investigation of novel techniques for the manipulation of the transverse beam dynamics and opens possibilities for realization of waveguides with complex transient geometries. Besides their intriguing physical picture, particular interest in dark spatial solitons (DSSs) is motivated by their ability to induce gradient optical waveguides in bulk self-defocusing NLM [6, 14, 15, 16, 17]. The only known truly 2-D DSSs are the OV solitons [1] whereas in one transverse spatial dimension the DSSs manifest themselves as self-supporting dark stripes [2].

On the other hand, the field of singular optics also knows dark (or grey) waves that slowly change their parameters even when they are generated from perfectly odd initial conditions. A classical example is the ring dark solitary wave [18, 19, 20, 21]. In their pioneering analysis [22], Nye and Berry conjectured that phase dislocations with a combination of a step- and screw-like phase profile (fractional vortex dipoles, FVDs) cannot exist. Nonetheless, indications for their existence were found [23, 24] for two interacting optical vortices of opposite topological charges. Moderate saturation of the medium's third-order nonlinearity enabled the suppression of the snake instability of crossed 1D dark solitons and the identification of 1-D fractional vortex dipoles (FVDs) of finite length [25, 26]. Later on, such FVDs with step-screw phase dislocations were experimentally generated under controllable initial conditions by computer-generated holograms [27]. Although two different schemes for directional coupling of signal beams by steering FVD beams were proposed in Kerr media with negative nonlinearities [28], the first successful experiment was conducted years later in a biased photorefractive medium with a positive nonlinearity [29]. The evolution of ordered structures of semi-infinite FVDs was studied for the first time [30] in a self-defocusing Kerr nonlinear medium. The results showed that depending on their phase profiles, four parallel semi-infinite FVDs aligned to initially form two dark stripes can evolve into two different cross-connects able to partially redirect collinearly- and perpendicularly-propagating probe optical beams at different branching efficiencies.

Let us here clarify the terminology adopted in this paper: The semi-infinite dark stripes (SIDSs) are in essence fractional vortex dipoles (FVDs) with one screw-like dislocation nested on the background while the second one is located far outside the background.

In this work we numerically analyze the evolution and interaction of 1-D dark spatial solitons (DSSs) and semi-infinite dark stripes (SIDSs) in a local self-defocusing Kerr nonlinear medium (NLM). The presented experimental results in the linear regime of propagation confirm that the SIDS-beam bending and fusion with the 1-D DSS predicted numerically for the nonlinear regime is due to the (suitably chosen) opposite phase semi-helicities of SIDS beam ends. Results for several interaction scenaria are shown - single DSS interacting with one, two, and four parallel SIDSs. Within a certain propagation distance along the NLM, the inherently restless ends of the semi-infinite dark stripes splice to the 1-D DSS to form structures resembling waveguide couplers/branchers. The ability of such 2-to-1 and 3-to-1 couplers to guide and merge probe waves is numerically investigated. In some cases the interaction of 1-D DSS and SIDSs steering away from the DSS is investigated for comparison too. A well pronounced modulational stability of the 1-D DSSs under strong symmetric background beam perturbations from decaying SIDSs is observed.

2. Numerical model and calibration

The pure 1-D phase dislocation of the dark beam is given by (see Fig. 1a)

$$\Phi^{1D}(y) = \begin{cases} +\Delta\Phi/2 & \text{for } y \leq 0 \\ -\Delta\Phi/2 & \text{for } y > 0. \end{cases} \tag{1}$$

The mixed (edge-screw, ES) phase dislocation of the FVD consists of a 1-D phase step of length $2b$, which ends with pairs of phase semi-spirals with opposite helicities. The phase profile of this mixed-type phase dislocation can be written in the form

$$\Phi^{FVD}(x,y) = \frac{\Delta\Phi}{2\pi}\left[\arctan\left(\frac{y}{x+b}\right) - \arctan\left(\frac{y}{x-b}\right)\right]. \tag{2}$$

In both equations $\Delta\Phi$ stands for the magnitude of the dislocation phase step and x and y denote the transverse Cartesian coordinates parallel and perpendicular to the dislocation. In order to keep the dark beam contrast and the refractive index modulation as high as possible, all data in this work refer to $\Delta\Phi = \pi$. The semi-infinite dark stripes (SIDSs) analyzed in this work (FVDs much longer than the background beam diameter) are modeled by shifting the respective amplitude and phase distributions to place one of the FVD beam ends initially at the center of the background beam while the second one is far outside the background (and the computational window). A surface plot of the phase of the semi-infinite dark stripe beam is shown in Fig. 1b. The slowly-varying electric field amplitude of each dark beam is assumed to be tanh-shaped of width a and, when centered on the background beam, of the form

$$E^J(x,y,z=0) = \sqrt{I_0}B(x,y)\tanh[r_{\alpha,\beta}(x,y)/a]\exp[i\Phi^J(x,y)], \tag{3}$$

where $J = 1D$ or $J = SIDS$. Here the effective coordinate $r_{\alpha,\beta}(x,y)$ is

$$r_{\alpha,\beta}(x,y) = [\alpha(x+\beta b)^2 + y^2]^{1/2}, \tag{4}$$

where for the 1-D dark beam $\alpha = 0$, while for the SIDS beam

$$\alpha = \begin{cases} 0 & \text{if } |x| \leq b \\ 1 & \text{and } \beta = -1 \text{ for } x > b. \\ 1 & \text{and } \beta = 1 \text{ for } x \leq -b \end{cases} \tag{5}$$

The finite background beam carrying the singular beams is chosen to be of a super-Gaussian form

$$B(x,y) = \exp\{-[(x^2+y^2)/w^2]^8\}, \tag{6}$$

and its width w is chosen to exceed more than 20 times the initial dark beam width a. The numerical simulations of the dark beam propagation along

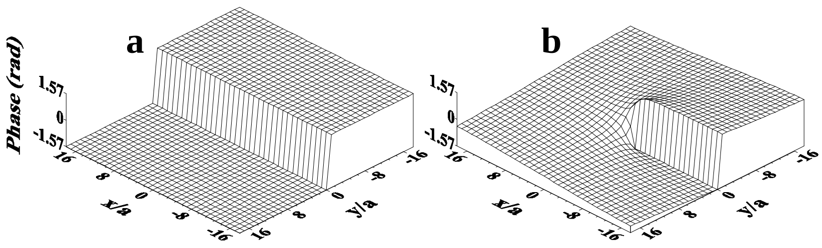

Figure 1: One-dimensional step phase dislocation (**a**) and semi-infinite edge-screw mixed phase dislocation of a semi-infinite dark stripe (**b**) described by Eq. 1 and Eq. 2, respectively.

the local Kerr NLM are carried out using the (2+1)-dimensional nonlinear Schrödinger equation

$$i\partial E/\partial(z/L_{Diff}) + (1/2)\Delta_T E - \gamma|E|^2 E = 0, \tag{7}$$

which accounts for the evolution of the slowly-varying optical beam envelope amplitude E under the combined action of nonlinearity and diffraction. Here Δ_T is the transverse part of the Laplace operator, $\gamma = L_{Diff}/L_{NL}$, and $L_{Diff} = ka^2$ and $L_{NL} = 1/(k|n_2|I)$ stand for the diffraction and nonlinear length of the dark beam respectively. The minus sign in Eq. 7 implies a self-defocusing nonlinearity, a necessary condition for dark spatial soliton ($\gamma = 1$) formation and for waveguiding by dark beams. In the above notations, k is the wave number inside the medium and I is the peak field intensity. The transverse spatial coordinates (x and y) are normalized to the odd dark beam width a. Eq. 7 was solved numerically by means of the split-step Fourier method with a computational window spanning over 1024×1024 grid points. As a standard test we modeled the formation of a fundamental 1-D dark spatial soliton up to $z = 5L_{NL}$ and compared it to the initial tanh-shaped 1-D dark beam profile. As shown in previous analyses of odd dark beams with mixed step-screw dislocations [27, 28], the background-beam intensity has a weak influence on the FVD beam's dynamics. Negative nonlinearity however is important for keeping the optically induced refractive index modulation gradients (e.g. dark beam profile and refractive index profile) steep, which is crucial for all-optical guiding, deflection, and switching of signal beams or pulses. The background beam intensity in the following simulations is kept equal to that needed to form this fundamental 1-D DSS ($I = I_{SOL}^{1D}$, i.e. $\gamma = 1$).

The incoming probe beams used in generating Fig. 8 are assumed to be Gaussian and of widths a, equal to the initial width of each of the dark beams. The numerical window containing the NLM is a cuboid, with the dark beams propagating along the z-coordinate, whereas the probe beams propagate and evolve along the coordinate x under the influence of diffraction and the induced refractive index modulation in the (y, z) plane. To model this, we solved the equation

$$i\partial S/\partial x + [1/(2L_{DS})](\partial^2/\partial y^2 + \partial^2/\partial z^2)S - |E|^2 S/L_{NL} = 0. \quad (8)$$

Here $L_{DS} = k_S a_S^2$ is the diffraction length of the bright probe beam of width a_S such that $L_{DS} = L_{Diff} = L_{NL}$. Since the evolution of the 1-D DSS and the SIDS(s) is followed up to $z = 4L_{NL}$ and from each simulation for the pump beams we stored 256 E-field amplitude and phase distributions, the computational grid for the probe beams spans over 256×256 grid points. Each probe beam enters well centered the induced waveguides at the wing of the background beam and at location $z = 1L_{NL}$.

3. Results and discussion

In the upper left frames in Fig. 2 we show the significant parts of the intensity (top left) and the phase profiles of a semi-infinite dark stripe. In this and in all other cases reported here, the desired phase distribution of the dark beam(s) is sent to a reflective liquid-crystal spatial phase modulator (HOLOEYE) and the linear beam evolution is experimentally followed up to $z = 3L_{Diff}$. In these measurements we used the attenuated output of a Ti:Sapphire laser with a central wavelength of $\lambda_c = 795nm$ and a charge-coupled device camera (Allied Vision Technologies Pike F-505B, 2452×2054 pix., $3.45\mu m$ pixel size). The diffraction length L_{Diff} is calibrated with respect to the spatial spreading (due to the diffraction) of the pure 1-D dark beam (see Fig. 3, lower left frame). All the presented linear measurements show that the scenaria of the interactions between the 1-D dark beam and the SIDSs are phase-dependent. Compensating for the diffraction, the self-defocusing nonlinearity keeps the dark beams narrow and the respective refractive index gradients steep, which is important for potential all-optical guiding applications (see Fig. 8). In the right column in Fig. 2 we show the nonlinear evolution of a single SIDS along the local self-defocusing Kerr NLM. As seen, the SIDS beam develops snake instability [31] near its end and one vortex becomes clearly separated from the bending rest of the dark stripe for $z > 3L_{NL}$. The respective phase profile (see e.g. the bottom right

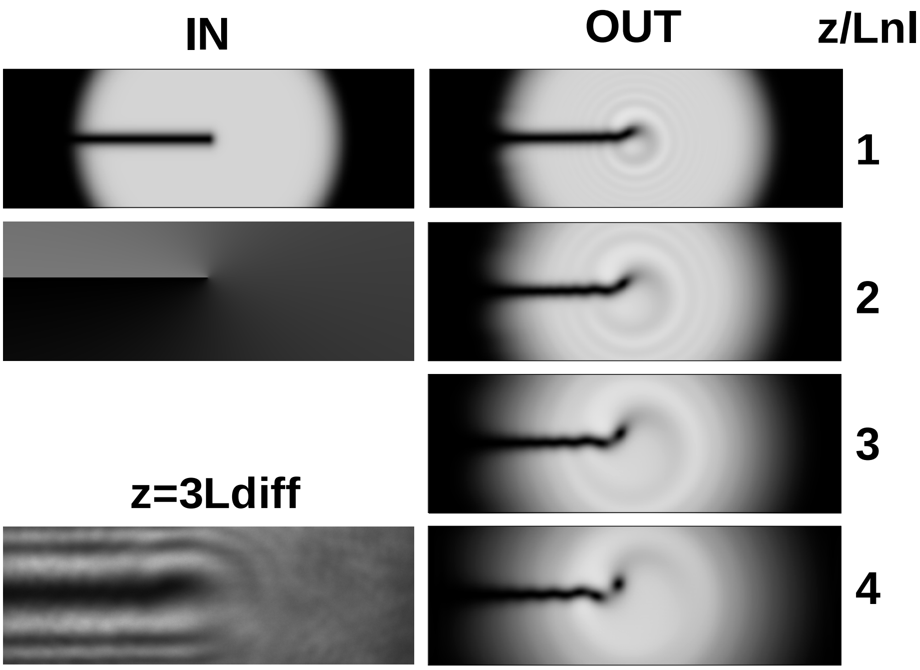

Figure 2: Upper left frames: Intensity (top left) and phase profiles of a semi-infinite dark stripe (SIDS) and experimentally recorded SIDS evolution up to $z = 3L_{Diff}$ (lower left frame). Right column: Nonlinear evolution of a single semi-infinite dark stripe along the local self-defocusing Kerr nonlinear medium (NLM). An animation (avi-file) of the SIDS beam evolution can be found in the supplementary material.

frame in Fig. 3 in [30]) shows that four vortices with alternating topological charges are formed, three of them with highly overlapping cores. (An animation (avi-file) of the SIDS beam evolution can be found in the supplementary material).

In Fig. 3, following the same style of presentation, we show the results obtained for a pure 1-D dark beam in the linear regime (lower left frame; $z = 3L_{Diff}$) and the 1-D dark spatial soliton formation up to $z = 4L_{NL}$ (right column). The inevitable nonlinear background beam broadening in the self-defocusing NLM is clearly visible.

In Fig. 4 we show the interaction between a 1-D dark beam and a single SIDS. The semi-infinite dark stripe is placed along the diameter of the background beam and the 1-D dark beam is shifted upwards as in generating Fig. 3. The intensity and phase profiles of the interacting (fusing) dark beams are shown in the upper left frames in Fig. 4. The SIDS beam bending towards the 1-D dark beam in the linear regime is clearly pronounced in the

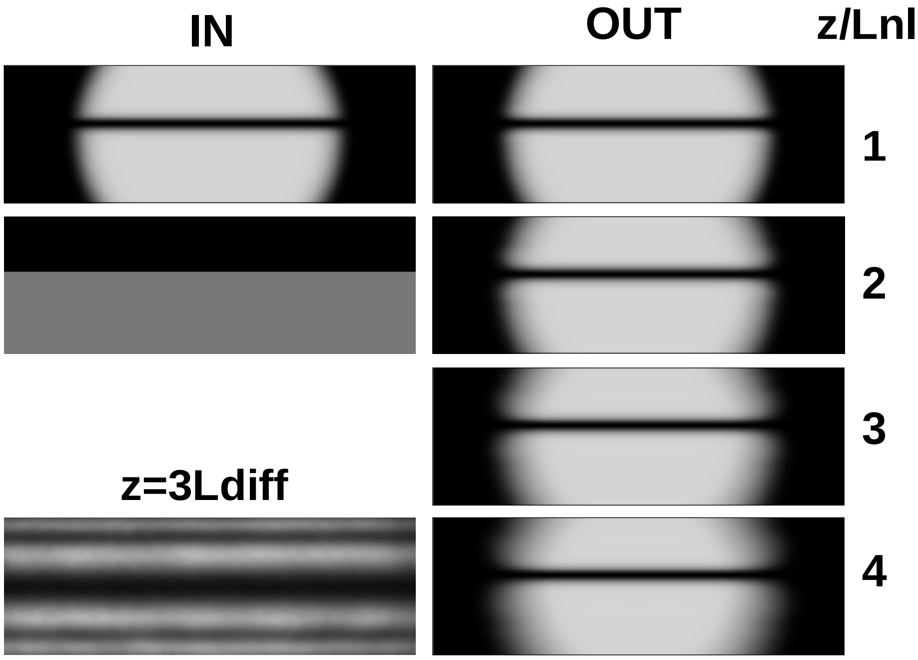

Figure 3: Upper left frames: Intensity (top left) and phase profiles of a one-dimensional odd dark beam (1-D ODB) and experimentally recorded 1-D ODB evolution up to $z = 3L_{Diff}$ (lowest left frame). Right column: Nonlinear evolution of a 1-D ODB along the local self-defocusing Kerr nonlinear medium demonstrating the formation of a 1-D dark spatial soliton (see also Fig. 2). An animation (avi-file) of the 1-D DSS formation can be found in the supplementary material.

experimentally recorded lower left frame ($z = 3L_{Diff}$). In the second column in Fig. 4 we show the evolution of the interacting dark beams along the NLM. Dark beam fusion is clearly observable near $z = 1L_{NL}$. Later on, the 1-D dark beam separates ($z = 2L_{NL}$) and is moved upwards by the repulsion from the SIDS beam. The bending end of the SIDS connects to the remaining unshifted part of the 1-D dark stripe. At larger nonlinear propagation distances both SIDS and 1-D dark beam develop snake instability near the background-beam center.

In contrast to Fig. 4, Fig. 5 presents the interaction between a 1-D dark beam and a pair of surrounding SIDSs. For suitably chosen and opposite helicities of the SIDS phases (left column, second frame), even in the linear regime of propagation the SIDS beams bend towards the central 1-D dark beam (experimentally recorded lower left frame; $z = 3L_{Diff}$). The same beam fusion in the nonlinear regime is clearly seen near $z = 1L_{NL}$. During

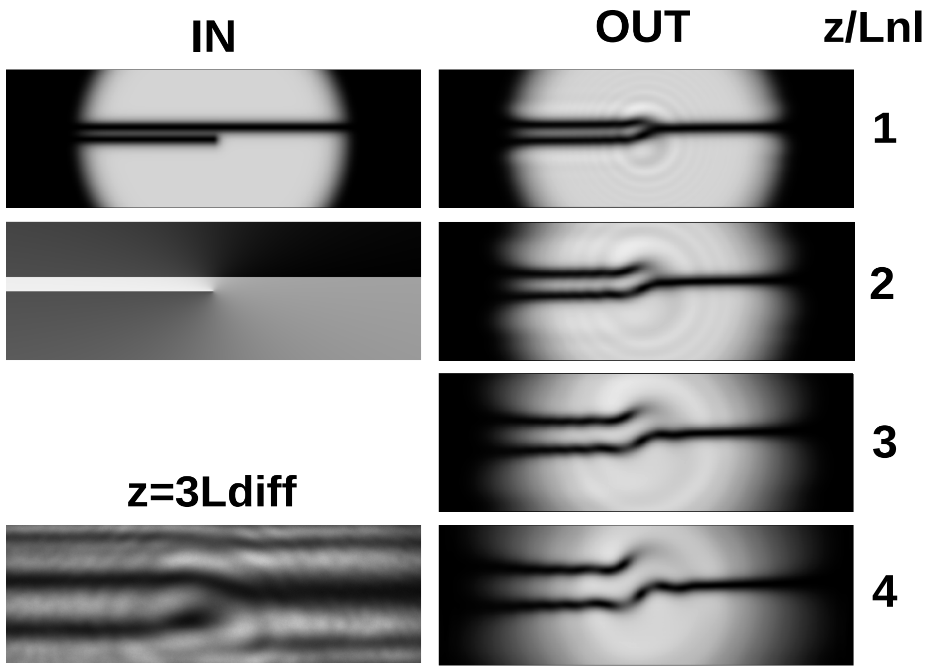

Figure 4: Upper left frames: Intensity (top left) and phase profiles of a 1-D ODB and a semi-infinite parallel SIDS and experimentally recorded dark beam evolution up to $z = 3L_{Diff}$ (lowest left frame). Right column: Nonlinear evolution of the dark beams along the local self-defocusing Kerr nonlinear medium demonstrating dark beam fusion. An animation (avi-file) can be found in the supplementary material.

propagation along the NLM the dark beam repulsion becomes stronger and the dark beam connections break up again. Hence, the proper nonlinear propagation distance for modeling the performance of a beam coupler/splitter based on this configuration is around $z = 1L_{NL}$.

The same conclusion can be drawn from the results shown in Fig. 6. Here we show the evolution and interaction of a 1-D dark beam and two pairs of surrounding SIDSs. The experimentally-recorded linear interaction structure is not as clear as in the preceding cases but the bending of the dark beam ends is indicative for the pair-wise bending of the ends of the SIDSs towards to the central 1-D dark beam. Similar pair-wise beam fusion to the 1-D dark beam in the nonlinear regime is clearly seen near $z = 1L_{NL}$. With increasing the propagation distance along the NLM, the outer-lying SIDS beams become detached from the fusion region (near $2 - 3L_{NL}$), followed by the inner-lying SIDSs (near $4L_{NL}$). After detaching from the fusion region,

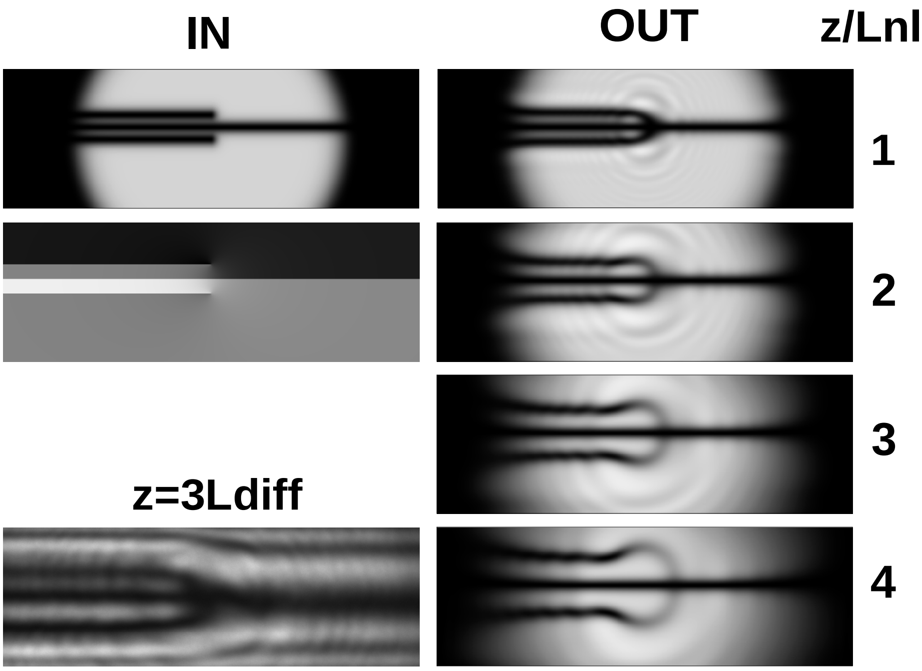

Figure 5: Upper left frames: Intensity (top left) and phase profiles of a 1-D ODB and a pair of side-lying semi-infinite parallel dark stripes and experimentally recorded dark beam evolution up to $z = 3L_{Diff}$ (lowest left frame). Right column: Nonlinear evolution of the dark beams along the local self-defocusing Kerr nonlinear medium demonstrating dark beam fusion ($z = 1L_{NL}$). An animation (avi-file) can be found in the supplementary material.

the SIDS beams develop a snake instability. It is worth mentioning that the 1-D dark beam exposed to strong symmetric perturbations clearly shows modulational stability and keeps propagating as a 1-D dark spatial soliton (see right columns in Figs. 5 and 6).

In Fig. 7 we show the interaction of a 1-D dark beam with a single SIDS (left column) and with a pair of surrounding SIDS (right column) when the initial phase(s) ofo the SIDS (Fig. 7, upper frames) are oriented in the opposite direction compared to the cases shown in Figs. 4 and 5. When a single SIDS is initially present on the background (Fig. 7, left column) its end bends away from the 1-D dark beam. Since the type of dark beam interaction is governed by topology, we observe dark beam repulsion (see the increasing distances between the parallel dark beams in the background-beam wing). The development of snake instability is clearly observed. The snake instability of the 1-D dark beam, however, is absent when the surrounding

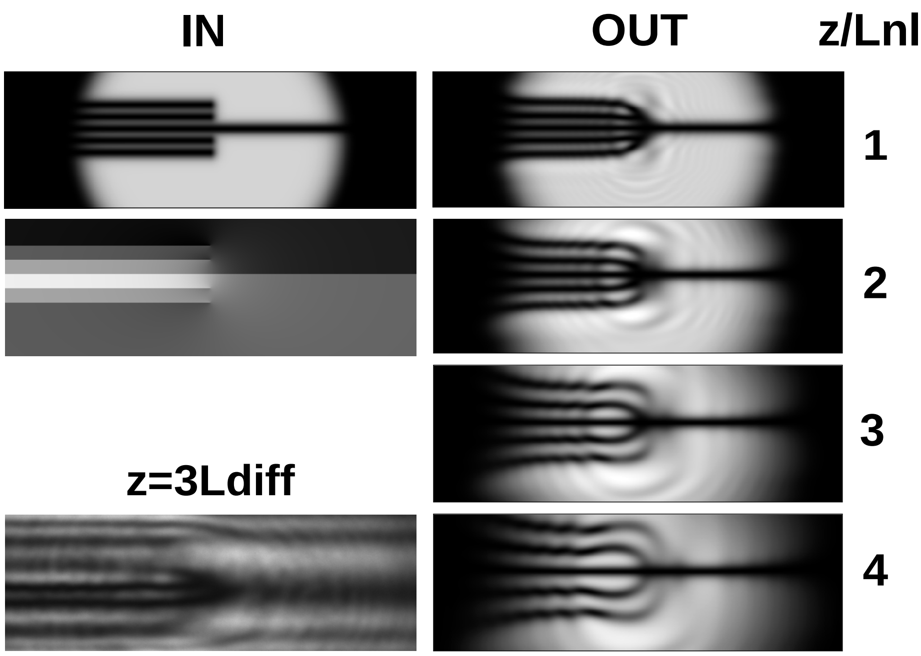

Figure 6: Upper left frames: Intensity (top left) and phase profiles of a 1-D dark beam and two pairs of semi-infinite parallel dark stripes and experimentally recorded dark beam evolution up to $z = 3L_{Diff}$ (lowest left frame). Right column: Nonlinear evolution of the dark beams along the local self-defocusing Kerr nonlinear medium demonstrating dark beam fusion (at $z = 1L_{NL}$). An animation (avi-file) can be found in the supplementary material.

pair of SIDS beams initially move away from the 1-D beam (Fig. 7, right column). We emphasize here the remarkable stability of the 1-D dark beam against such strong symmetric perturbations. The detailed analysis showed that under such perturbations it essentially evolved like 1-D dark spatial solitons.

Summarizing the findings up to this point, we may say that a single DSS interacting (eventually) with one or two parallel SIDSs can form 1-to-1, 2-to-1 and 3-to-1 couplers to guide and merge probe waves. We analyzed the two non-trivial cases numerically by solving Eq. 8. In Fig. 8a we show a schematic of the interaction geometry inside the NLM. The weak in-phase bright probe beams (the arrows in Fig. 8a) enter well centered the dark-beam-induced waveguides at $z = 1L_{NL}$ (see the upper frames in Figs. 4 and 5) and propagate perpendicularly to the background beam carrying the dark structures. The obtained results for the probe beams are presented in Fig. 8b,c as beam cross-

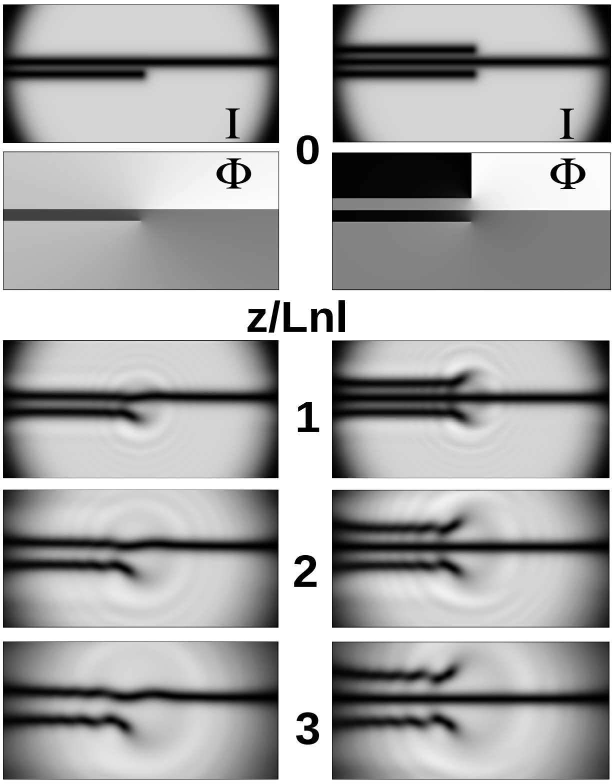

Figure 7: Upper frames: Initial intensity (first row) and phase profiles (second row) of a 1-D dark beam and of syde-lying single (left) and pair of SIDS (right) which ends later steer away from the 1-D dark beam. Lower block of frames: Nonlinear evolution of the dark beams along the NLM. Note the presence (left lower frames) and absence (lower right frames) of modulational instability of the 1-D dark beam in dependence of the absence/presence of symmetry of the transverse perturbations.

sections. The curves with hollow circles denote the probe beam profiles at the exit of the interaction region in the pure linear regime of propagation. The red solid curves represent the output probe beam profiles in the nonlinear regime. Because of the two interacting dark beams in the 2-to-1 coupler, there is a small shift between the location of the center of mass of the incoming probe beams (dashed curves in Fig.8b) with respect to the combined output probe beam in the nonlinear regime (red solid curve). This is due to the initial asymmetry (one 1-D dark beam and one side-lying SIDS) resulting in a waveguide moving in the transverse direction. The symmetric dark beam disposition in the case of the 3-to-1 coupler ensures transverse stationarity of the waveguides (at least up to $z = 1L_{NL}$). That is why the center of mass of the input (Fig. 8c, dashed curve) and of the output probe beams (red solid curve) coincide. Assuming that *each* probe beam carries initially one unit of energy (total of two and three units of probe wave energy for the two respective cases considered), at the exit of the 2-to-1 nonlinear coupler the probe wave carries 1.04 units of energy, i.e. the nonlinear output coupling efficiency is $\sim 52\%$. In the purely linear regime only 26% of the total input energy is transferred to the same output virtual channel (of a width a equal to the width of the input dark beam). The calculations for the 3-to-1 nonlinear coupler showed that the output probe wave carries 1.86 units of energy of the total 3 units of input energy (efficiency $\sim 62\%$). In the purely linear regime the output coupling efficiency is 36% only. This moderate coupling efficiency is due to the lack of effective refractive-index modulation (and induced waveguiding) for the probe beams along the z-axis (see Fig. 8a). Still being far from discussing particular practical applications, the desirable high-efficiency coupling/splitting of probe beams by interacting 1-D dark beams and semi-infinite dark beams seems feasible and the presented results provide a reasonable first step for further optimization of such interaction schemes.

4. Conclusion

The presented results show that the interaction between infinite 1-D dark beams and semi-infinite dark stripes (SIDSs) is governed by their spatial phases. The medium's nonlinearity, when negative, smoothes out the oscillations on the background beam due to the SIDS beam bending and dark beam repulsion. In view of potential all-optical guiding/switching applications, the negative nonlinearity has the important role to keep the dark beams narrow and the respective refractive index modulation gradients steep. The news here can be summarized as follows: *i*) The known repulsion between coherent 1-D dark beams (solitons) holds true also for the interaction between a 1-D dark beam and semi-infinite FVD(s). The bending end of the FVD(s) develops a snake instability; *ii*) Steering SIDSs can split an infinite 1-D dark beam into two new SIDSs (Fig. 4; lower two frames in the middle column). Eventually, the input SIDS beam end(s) can connect to the 1-D beam or to the one of the newly born SIDSs to form an optically-induced nonlinear coupler (see Figs. 4-6) or a curved waveguide (see Fig. 4); *iii*) One dimensional dark spatial solitons remain stable under strong symmetric spatial perturbations induced by SIDSs. Numerical calculations show reasonably high efficiencies for couplers that consist of interacting 1-D dark beams and semi-infinite dark beams, subject to optimization and further investigation of these all-optical guiding and switching schemes.

5. Acknowledgments

This work was supported by the DFG in the framework of Forschergruppe 532 "Nichtlineare raum-zeitliche Dynamik in dissipativen und diskreten optischen Systemen" and by the Science Fund of Sofia University (Bulgaria). A.D. dedicates his work in loving memory to his dear friend and biologist Mrs. Jolana Koleva who passed away so unexpectedly.

6. Captions for the figures

Fig.1 – One-dimensional step phase dislocation (**a**) and semi-infinite edge-screw mixed phase dislocation of a semi-infinite dark stripe (**b**) described by Eq. 1 and Eq. 2, respectively.

Fig.2 – Upper left frames: Intensity (top left) and phase profiles of a semi-infinite dark stripe (SIDS) and experimentally recorded SIDS evolution up to $z = 3L_{Diff}$ (lower left frame). Right column: Nonlinear evolution of a single semi-infinite dark stripe along the local self-defocusing Kerr nonlinear medium (NLM). An animation (avi-file) of the SIDS beam evolution can be found in the supplementary material.

Fig.3 – Upper left frames: Intensity (top left) and phase profiles of a one-dimensional odd dark beam (1-D ODB) and experimentally recorded 1-D ODB evolution up to $z = 3L_{Diff}$ (lowest left frame). Right column: Nonlinear evolution of a 1-D ODB along the local self-defocusing Kerr nonlinear medium demonstrating the formation of a 1-D dark spatial soliton (see also Fig. 2). An animation (avi-file) of the 1-D DSS formation can be found in the supplementary material.

Fig.4 – Upper left frames: Intensity (top left) and phase profiles of a 1-D ODB and a semi-infinite parallel SIDS and experimentally recorded dark beam evolution up to $z = 3L_{Diff}$ (lowest left frame). Right column: Nonlinear evolution of the dark beams along the local self-defocusing Kerr nonlinear medium demonstrating dark beam fusion. An animation (avi-file) can be found in the supplementary material.

Fig.5 – Upper left frames: Intensity (top left) and phase profiles of a 1-D ODB and a pair of side-lying semi-infinite parallel dark stripes and experimentally recorded dark beam evolution up to $z = 3L_{Diff}$ (lowest left

frame). Right column: Nonlinear evolution of the dark beams along the local self-defocusing Kerr nonlinear medium demonstrating dark beam fusion ($z = 1L_{NL}$). An animation (avi-file) can be found in the supplementary material.

Fig.6 – Upper left frames: Intensity (top left) and phase profiles of a 1-D dark beam and two pairs of semi-infinite parallel dark stripes and experimentally recorded dark beam evolution up to $z = 3L_{Diff}$ (lowest left frame). Right column: Nonlinear evolution of the dark beams along the local self-defocusing Kerr nonlinear medium demonstrating dark beam fusion (at $z = 1L_{NL}$). An animation (avi-file) can be found in the supplementary material.

Fig.7 – Upper frames: Initial intensity (first row) and phase profiles (second row) of a 1-D dark beam and of syde-lying single (left) and pair of SIDS (right) which ends later steer away from the 1-D dark beam. Lower block of frames: Nonlinear evolution of the dark beams along the NLM. Note the presence (left lower frames) and absence (lower right frames) of modulational instability of the 1-D dark beam in dependence of the absence/presence of symmetry of the transverse perturbations.

Fig.8 – **a)** Schematic view of the background beam carrying the 1-D dark beam and two SIDSs inside the nonlinear medium (NLM) with the used notations of the coordinate system axes. The dark beams propagate along the z-axis, the probe beams - perpendicularly, along the x-axis, entering the NLM at $z = 1L_{NL}$. The tiny (color) lines cross the $x - y$-plane approximately at the position of the background beam propagation axis. **b)** and **c)**: Coupling of two **b)** and three input probe beams **c)** into a single output channel by all-optical guiding structures formed by fusing 1-D dark beam and a singlel SIDS (Case **b)**; see Fig. 4 at $z = 1L_{NL}$) and by fusing 1-D dark beam and a pair of surrounding SIDSs (Case **c)**, see Fig. 5 at $z = 1L_{NL}$). Dashed curves - cross-sections of the input probe beams. Hollow circles - output probe beams in the linear regime. Red solid curves - cross-sections of the output probe beams in the nonlinear regime.

References

[1] G. A. Swartzlander, Jr., C. T. Law, Phys. Rev. Lett. 69 (1992) 2503–2506.

[2] G. Allan, S. Skinner, D. Andersen, A. Smirl, Opt. Lett. 16 (1991) 156–158.

[3] Yu. S. Kivshar, B. Luther-Davies, Phys. Rep. 298 (1998) 81–197.

[4] M. S. Soskin, M. V. Vasnetsov, Prog. in Optics 42 (2001) 219–276.

[5] Yu. S. Kivshar, G. P. Agrawal, Optical Solitons: From Fibers to Photonic Crystals (Academic Press, San Diego, 2003).

[6] G. I. Stegeman, M. Segev, Science 286 (1999) 1518–1523.

[7] D. Rozas, C. T. Law, G. A. Swartzlander, Jr., J. Opt. Soc. Am. B 14 (1997) 3054–3065.

[8] P. Hansinger, A. Dreischuh, G. G. Paulus, Opt. Commun. 282 (2009) 3349–3355.

[9] D. Neshev, A. Dreischuh, M. Assa, S. Dinev, Opt. Commun. 151 (1998) 413–421.

[10] A. Dreischuh, D. N. Neshev, D. E. Petersen, O. Bang, W. Krolikowski, Phys. Rev. Lett. 96 (2006) art. 043901.

[11] A. Dreischuh, S. Chervenkov, D. Neshev, G. G. Paulus, H. Walther, J. Opt. Soc. Am. B 19 (2002) 550–556.

[12] A. S. Desyatnikov, N. Sagemerten, R. Fisher, B. Terhalle, D. Træger, D. N. Neshev, A. Dreischuh, C. Denz, W. Krolikowski, Yu. S. Kivshar, Opt. Express 14 (2006) 2851–2863.

[13] R. De La Fuente, A. Barthelemy, C. Froehly, Opt. Lett. 16 (1991) 793–795.

[14] A. W. Snyder, A. P. Sheppard, Opt. Lett. 18 (1993) 482–484.

[15] E. A. Ostrovskaya, Yu. S. Kivshar, Opt. Lett. 23 (1998) 1268–1270.

[16] A. H. Carlsson, J. N. Malmberg, E. A.Ostrovskaya, T. J. Alexander, D. Anderson, M. Lisak, and Yu. Kivshar, Opt. Lett. 25 (2000) 660–662.

[17] C. T. Law, X. Zhang, G. A. Swartzlander, Jr., Opt. Lett. 25 (2000) 55–57.

[18] Yu. S. Kivshar, X. Yang, Phys. Rev. E 50 (1994) R40–R43.

[19] Yu. S. Kivshar, X. Yang, Chaos, Solitons and Fractals 4 (1994) 1745–1758.

[20] D. Neshev, A. Dreischuh, V. Kamenov, I. Stefanov, S. Dinev, W. Fließer, L. Windholz, Appl. Phys. B 64 (1997) 429–433.

[21] A. Dreischuh, D. Neshev, G. G. Paulus, F. Grasbon, H. Walther, Phys. Rev. E 66 (2002) 066611(1–7).

[22] J. F. Nye, M. V. Berry, Proc. R. Soc. London A 336 (1974) 165–190.

[23] V. Bazhenov, M. Soskin, M. Vasnetsov, J. Mod. Opt. 39 (1992) 985–990.

[24] I. Basistiy, V. Bazhenov, M. Soskin, M. Vasnetsov, Opt. Commun. 103 (1993) 422–428.

[25] A. Dreischuh, G. G. Paulus, F. Zacher, Appl. Phys. B 69 (1999) 107–111.

[26] A. Dreischuh, G. G. Paulus, F. Zacher, I. Velchev, Appl. Phys. B 69 (1999) 113–117.

[27] A. Dreischuh, D. Neshev, G. G. Paulus, H. Walther, J. Opt. Soc. Am. B 17 (2000) 2011–2016.

[28] D. Neshev, A. Dreischuh, G. G. Paulus, H. Walther, Appl. Phys. B 72 (2001) 849–854.

[29] G. Maleshkov, D. N. Neshev, A. Dreischuh, Phys. Rev. A 80 (2009) 053828(1–5).

[30] G. Maleshkov, P. Hansinger, N. Dimitrov, A. Dreischuh, and G. G. Paulus, Opt. Commun. 285 (2012) 3529–3534.

[31] V. Tikhonenko, J. Christou, B. Luther-Davies, Yu. S. Kivshar, Opt. Lett. 21 (1996) 1129–1131.

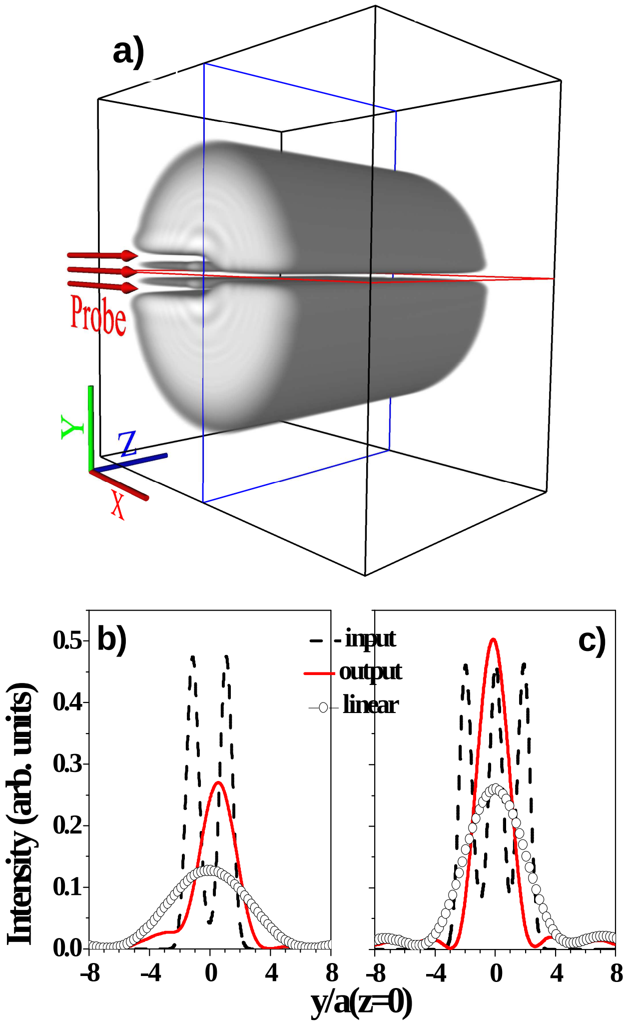

Figure 8: **a)** Schematic view of the background beam carrying the 1-D dark beam and two SIDSs inside the nonlinear medium (NLM) with the used notations of the coordinate system axes. The dark beams propagate along the z-axis, the probe beams - perpendicularly, along the x-axis, entering the NLM at $z = 1L_{NL}$. The tiny (color) lines cross the $x - y$-plane approximately at the position of the background beam propagation axis. **b)** and **c)**: Coupling of two **b)** and three input probe beams **c)** into a single output channel by all-optical guiding structures formed by fusing 1-D dark beam and a single SIDS (Case **b)**; see Fig. 4 at $z = 1L_{NL}$) and by fusing 1-D dark beam and a pair of surrounding SIDSs (Case **c)**, see Fig. 5 at $z = 1L_{NL}$). Dashed curves - cross-sections of the input probe beams. Hollow circles - output probe beams in the linear regime. Red solid curves - cross-sections of the output probe beams in the nonlinear regime.